metals

MDPI

Article

Preparation of Doped Iron Phosphate by Selective Precipitation of Iron from Titanium Dioxide Waste Acid

Weiguang Zhang [1,2], Ting-an Zhang [1,2,*], Liuliu Cai [1,2], Guozhi Lv [1,2] and Xuejiao Cao [1,2]

[1] School of Metallurgy, Northeastern University, Shenyang 100819, China; zhangwg@smm.neu.edu.cn (W.Z.); m18712707230@163.com (L.C.); lvgz@smm.neu.edu.cn (G.L.); xuejiao628@163.com (X.C.)

[2] Key Laboratory of Ecological Metallurgy of Multi-metal Intergrown Ores of Ministry of Education, Shenyang 100819, China

* Correspondence: zta2000@163.net; Tel.: +86-24-8368-6283

Received: 30 April 2020; Accepted: 11 June 2020; Published: 14 June 2020

Abstract: In view of the current situation where the acid resources and valuable components in titanium dioxide waste acid cannot be effectively extracted and are prone to secondary pollution, the research team proposed a new technology of step extraction and comprehensive utilization of titanium dioxide waste acid. In this paper, the preparation of doped iron phosphate from waste acid by selective precipitation was studied. The thermodynamics of selective precipitation, the effect of the reaction temperature, the initial pH value, the molar ratio of P/Fe, and the dispersant on the precipitation process were investigated in detail. The thermodynamics results show that iron(II) in titanium dioxide waste acid is oxidized and is preferentially precipitated with phosphoric acid to form iron(III) phosphate, when compared with other impurity ions. The experimental results show that the optimal precipitation condition is a temperature of 60 °C, an initial pH value of 2.5, an optimal P/Fe molar ratio of 1.1, and a dispersant polyethylene glycol at 5 mL (Per 50 mL of waster acid). After calcination, the precipitate mainly consists of iron phosphate and a small amount of aluminum phosphate. Meanwhile, the utilization ratios of iron and phosphorus were 98.81% and 98.39%, respectively. Moreover, the mass percentage of Fe_2O_3 and P_2O_5 and the molar ratio of Fe/P were 99.13% and 1.03, which basically met the requirements of the iron phosphate precursor.

Keywords: titanium dioxide waste acid; selective precipitation; iron phosphate

1. Introduction

Titanium dioxide, as an important white inorganic pigment, is produced by chlorination and sulfuric acid decomposition. In China, 95% of titanium dioxide is produced by the sulfuric acid decomposition method due to the low grade of titanium resources and the easy operation. The process route is shown in Figure 1 [1,2]. However, a large amount of waste acid will be produced in the hydrolysis process for preparing titanium dioxide. Generally, 8–10 tons of waste acid will be produced in the production of 1 t of titanium dioxide, 25–35% of which will be reused, and the actual discharged waste acid is 6–6.5 tons. According to the current capacity of titanium dioxide in China, the waste acid discharged each year amounts to millions of tons [3].

Titanium dioxide waste acid contains 200 g/L sulfuric acid, 30 g/L iron(II), trace scandium, and many other valuable components. If discharged directly, it can pollute the water body and acidify the soil, then destroy the ecological environment and affect the production and development of industry and agriculture [4].

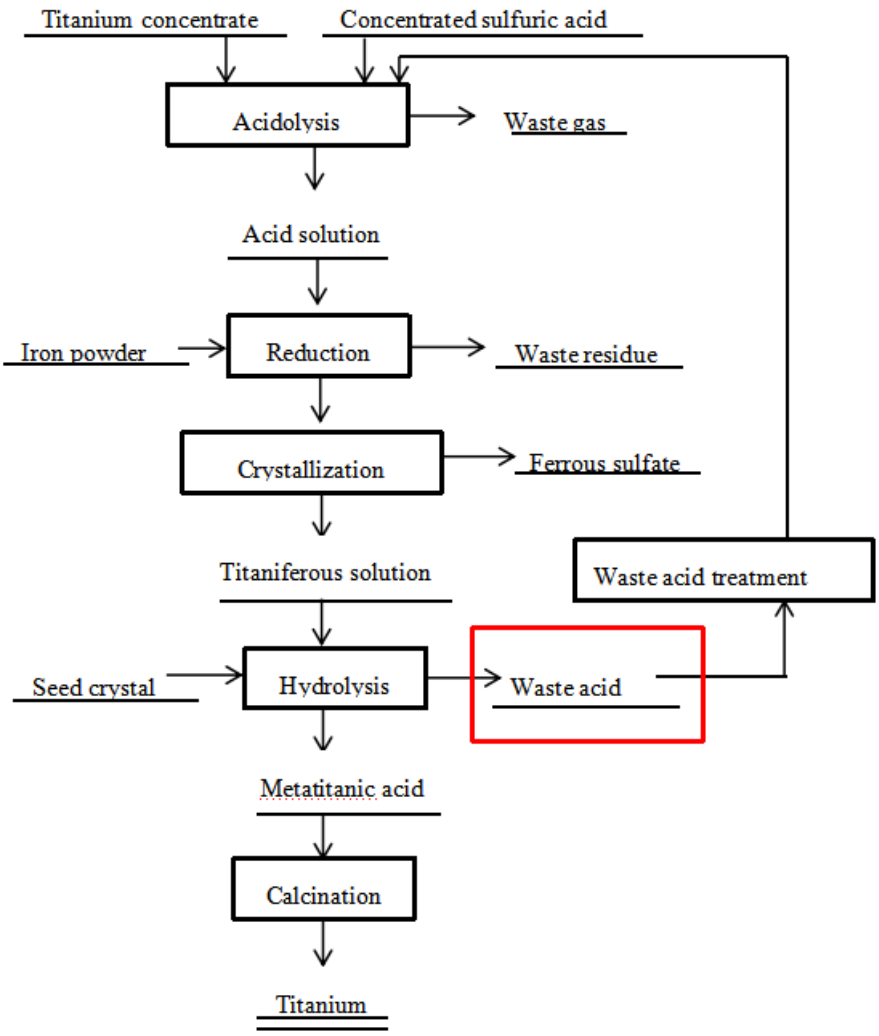

Figure 1. Technological route of titanium dioxide production by sulfuric acid decomposition.

In the titanium white production enterprise by the sulfuric acid process, the treatment methods of titanium dioxide waste acid mainly include vacuum concentration, lime neutralization, and the leaching of mineral. The main problem of vacuum concentration and lime neutralization is the high treatment cost. According to the lime neutralization method with the lowest treatment cost, the treatment cost of each ton of titanium dioxide waste acid is more than RMB 60 yuan. Another problem of the neutralization method is that the produced neutralization slag easily causes secondary pollution [2,5,6]. Moreover, titanium dioxide waste acid can be directly used for the acid leaching of minerals. Although the waste acid resources can be utilized, the valuable components in the waste acid are difficult to extract and utilize, which wastes the valuable metal resources. In conclusion, the common problems of the three methods are that the acid resources in titanium dioxide waste acid, as well as the valuable metal scandium and iron, have not been effectively extracted and utilized.

Based on this, our research team proposed a new method for the step extraction of valuable components from titanium dioxide waste acid. Additionally, related patents have been applied [7–9]. First, the trace scandium in titanium dioxide waste acid is selectively extracted by the solvent extraction method [10]. Furthermore, raffinate containing divalent iron can be used to prepare iron phosphate or doped iron phosphate precursor by adding a precipitant containing phosphorus, which is the research content of this paper. Then, the acid resource in the waste acid can be used in the acidic leaching process of minerals to realize the comprehensive utilization of acid resources [11,12].

In recent years, lithium iron phosphate, as the cathode material of lithium-ion batteries, has become one of the most promising cathode materials for lithium-ion batteries due to the advantage of having a high theoretical specific capacity (170 mAh/g), good cycle performance, good thermal stability, low price, and environmental friendliness [13–15]. At present, most of the iron sources for the preparation of lithium iron phosphate are analytical pure iron salts, mainly including ferrous oxalate, ferrous acetate, ferrous sulfate, iron sulfate, iron nitrate, iron phosphate, iron oxide, etc. The price of these analytical pure iron salts is relatively high, and some doping elements (such as Mg, Mn, Al, Ti, etc.) which are beneficial to their electrochemical properties need to be added when they are used to prepare high-performance lithium iron phosphate [16–19]. These doping elements happen to exist in the titanium dioxide waste acid. Therefore, the preparation of the precursor of lithium iron phosphate from titanium dioxide waste acid is a good choice for both the raw material of lithium iron phosphate and the comprehensive utilization of titanium dioxide waste acid. As the precursor of lithium phosphate for batteries, the requirements of iron phosphate are mainly based on the chemical industry standard of the People's Republic of China (Hg/T 4701-2014) – «iron phosphate for battery». The technical requirements in the standard are: Fe = 29.0–30.0 wt%, P = 16.2–17.2 wt%, molar ratio of Fe:P = 0.97–1.02, D_{50} = 2–6 μm.

In this paper, combined with the thermodynamic difference of the phosphate precipitation between iron and other metals in titanium dioxide waste acid, the process of preparing iron phosphate or doped iron phosphate by the selective precipitation of waste acid after scandium extraction was investigated in detail. The effects of the reaction temperature, pH value of solution, molar ratio of P/Fe, and dispersant on the precipitation of iron phosphate were investigated.

In order to realize the industrial application of this process, the precipitant containing phosphorus is a key research material. The world's phosphorus resources are in short supply. According to the proven phosphorus reserves and mining speed, the world's existing phosphorus resources can only be maintained for 50–100 years. Therefore, the extraction and reuse of phosphorus in secondary resources containing phosphorus will be our next work focus.

From literature research, it can be seen that the secondary phosphorus resources from three industries have the prospect of extracting and reusing phosphorus.

(1) Chemical industry. In the process of phosphoric acid production, chemical etching, electrochemical polishing, phosphoric acid phosphating, chemical cleaning, pesticide production, and other industrial production, a large amount of waste liquid containing phosphoric acid will be produced every year. This waste liquid often contains high concentrations of phosphoric acid, which involves mature methods for utilizing phosphoric acid, including solvent extraction, membrane separation, regeneration, distillation, etc. In addition, the by-product of the phosphorus chemical industry, ferrophosphorus slag (the mass fraction of phosphorus and iron is generally more than 80%), is also a potential secondary resource containing phosphorus [20–22].

(2) Metallurgical industry. Several hundred million tons of converter slag discharged every year in China are generally in a state of storage. Among them, phosphorus is considered to be the most valuable and promising element. The content of P_2O_5 is usually in the range of 3–10%, containing a huge amount of phosphorus resources and being equivalent to 20% of the total amount of P_2O_5 in China's annual phosphorus mining. Therefore, the extraction and recovery of phosphorus resources in steel slag can greatly alleviate the dependence of industrial production on phosphorus ore [23].

(3) Power battery industry. Following the advent of the service life of power batteries, the amount of waste power batteries in China will reach more than 2.0 million tons in 2020, which is not only a huge secondary resource containing lithium, but also a good secondary resource containing phosphorus. Therefore, it is very important to recover and treat the phosphorus resources in waste lithium iron phosphate power batteries [24].

2. Methodology

2.1. Materials

The titanium dioxide waste acid for the experiment was prepared by dissolving ferrous sulfate, vanadyl sulfate, magnesium sulfate, manganese sulfate, calcium hydroxide, and aluminum sulfate in deionized water. All the reagents were analytical grade, including hydrogen peroxide and phosphoric acid. The deionized water used in the experiments was produced by a water purification system.

2.2. Experimental Methods

The process route "step extraction of valuable components from titanium dioxide waste acid" is shown in Figure 2. Our research work is mainly focused on the selective precipitation of iron.

All experiments were performed in a glass beaker with a thermostatic mixing water bath pot. A predetermined amount of titanium dioxide waste acid was added to the beaker at constant stirring. Subsequently, the pH value of the solution was adjusted with sulfuric acid and ammonia. The solution was heated to a predetermined temperature.

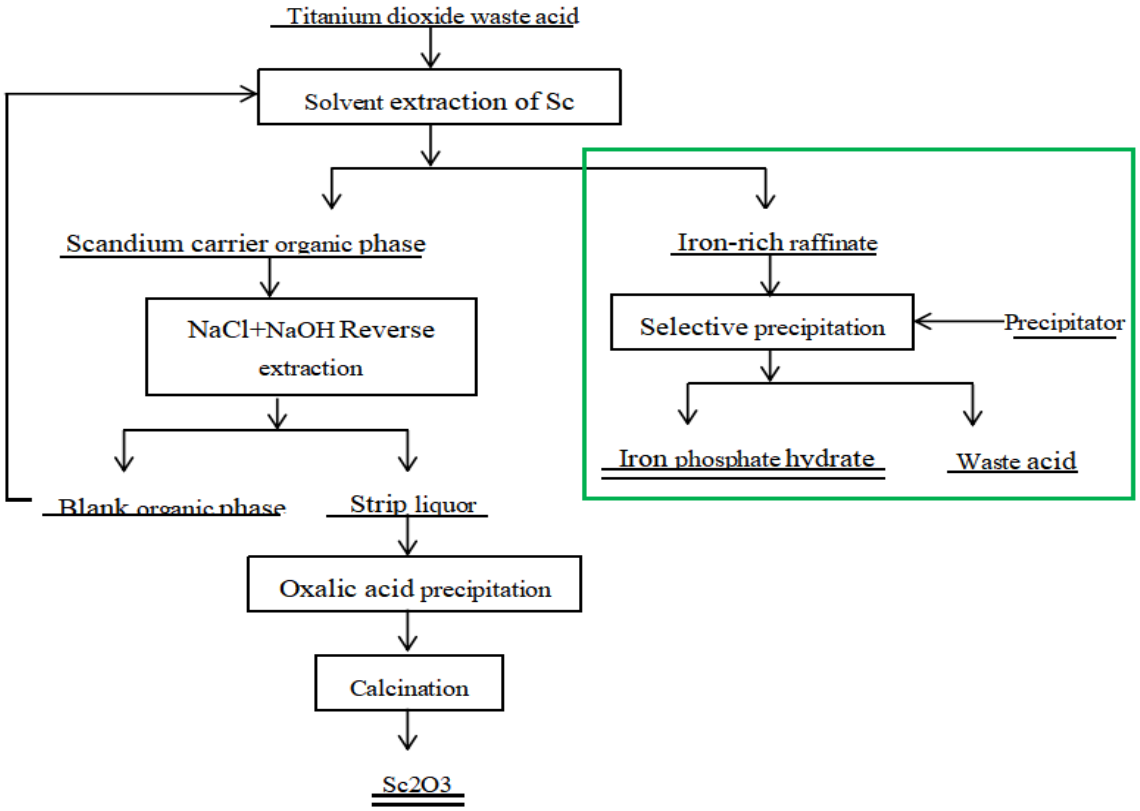

Figure 2. Technological route for the step extraction of valuable components from titanium dioxide waste acid.

The experiment was divided into the following two steps: first, quantitative hydrogen peroxide was added to the beaker to ensure the complete oxidation of Fe^{2+} in titanium dioxide waste acid to Fe^{3+}; Next, with the addition of the phosphoric acid solution, Fe^{3+} in titanium dioxide waste acid preferentially formed the iron phosphate precipitate. After the required reaction time, the filtrate was separated from the precipitation through vacuum filtration. The remaining residue was roasted at 700 °C for 8 h in order to determine the phase of the precipitate. The reaction equation is as follows:

$$2FeSO_4 + H_2O_2 + 2H_3PO_4 = 2FePO_4 + 2H_2O + 2H_2SO_4$$

The percent yield of P or Fe was calculated using the following formula:

$$\lambda = \frac{m \times \eta}{V \times C} \times 100\% \quad (1)$$

where λ is the percent yield of P or Fe, %; m is the quality of the iron phosphate precipitation, g; η is the mass fraction of P or Fe in the iron phosphate precipitation; V is the volume of titanium dioxide waste acid, mL; and C is the concentration of iron and phosphorus in titanium dioxide waste acid, g/L.

The relative purity of the iron phosphate is defined as the mass percentage of Fe_2O_3 and P_2O_5 in the precipitated product, which is calculated using the following formula:

$$\theta = \frac{m_{(P_2O_5+Fe_2O_3)}}{m} \times 100\% \quad (2)$$

where θ is the proportion of phosphorus pentoxide and iron oxide in the precipitation, which is defined as the purity of the iron phosphate, %; $m_{(P_2O_5+Fe_2O_3)}$ refers to the mass sum of phosphorus pentoxide and iron oxide in the precipitation, g; and m is the mass of the precipitation product, g.

2.3. Measurement and Characterization

The crystalline phases of the iron phosphate precipitation were detected by X-Ray Diffraction of (XRD, D2-PHASER, Brooke, Saarbrucken, Germany). The samples were characterized by scanning electron microscopy (JSM-6360LV, JEOL, EDAX company, Philadelphia, PA, USA). Mass fractions of metals in the iron phosphate precipitation were analyzed by an X-ray fluorescence spectrometer (XRF, Rigaku corporation, Tokyo, Japan). The particle size distributions of the iron phosphate precipitation were measured by Laser particle size meter (Type3000) (Malvern, London, UK).

3. Results and Discussion

3.1. Technology Principle–Fundamentals of Thermodynamic Analysis

3.1.1. Thermodynamic Data and Calculation of Thermodynamic Equilibrium

The chemical composition of titanium dioxide waste acid is shown in the Table 1.

Table 1. Composition of titanium dioxide waste acid used in the experiment.

Element	Fe	V	Mg	Mn	Ca	Al
Concentration/g·L^{-1}	37.64	0.41	5	2.15	0.23	1.52

There are many kinds of metal ions such as Mn^{2+}, Mg^{2+}, Ca^{2+}, Al^{3+}, Fe^{2+}, and a large number of SO_4^{2-} ions in the reaction system of titanium dioxide waste acid and phosphoric acid. With the gradual increase of pH, all kinds of phosphate and hydroxide precipitates are produced gradually. The solubility product of all orthophosphates ($M_X(PO_4)y$) and hydroxides ($M_X(OH)_y$) that may exist in the system are shown in Table 2 below.

Taking [Fe] in the system as an example, the drawing method of the lg[M^{n+}]-pH diagram was introduced in detail [26–29]. Moreover, the thermodynamic data of the relevant reactions are listed in Table 3.

Table 2. Solubility product of precipitates that may appear in the reaction system (298.15 K).

Substance	State	Solubility Product Constant [25]
$Fe_3(PO_4)_2{\cdot}H_2O$	solid	$Ksp = 9.94 \times 10^{-29}$
$Mn_3(PO_4)_2{\cdot}nH_2O$	solid	$Ksp = 6.13 \times 10^{-32}$
$AlPO_4{\cdot}1.5H_2O$	solid	$Ksp = 3.5 \times 10^{-21}$
$Mg_3(PO_4)_2{\cdot}8H_2O$	solid	$Ksp = 6.31 \times 10^{-26}$
$Fe_3(PO_4)_2$	solid	$Ksp = 1.3 \times 10^{-22}$
$Ca_3(PO_4)_2$	solid	$Ksp = 2 \times 10^{-29}$
$Fe(OH)_3$	solid	$Ksp = 2.79 \times 10^{-39}$
$Mn(OH)_2$	solid	$Ksp = 1.9 \times 10^{-13}$
$Al(OH)_3$	solid	$Ksp = 1.3 \times 10^{-33}$
$Mg(OH)_2$	solid	$Ksp = 5.61 \times 10^{-12}$
$Ca(OH)_2$	solid	$Ksp = 5.5 \times 10^{-6}$

Table 3. Chemical equations and expanded forms in the system [25].

Equilibrium Reactions	Equilibrium Constants (lg*K*)	Mathematical Relationships
$Fe^{3+} + OH^- = FeOH^{2+}$	11.87	$[FeOH^{2+}] = 10^{11.87}[Fe^{3+}][OH^-]$
$Fe^{3+} + 2OH^- = Fe(OH)_2{}^+$	21.17	$[Fe(OH)_2{}^+] = 10^{21.17}[Fe^{3+}][OH^-]^2$
$Fe^{3+} + 3OH^- = Fe(OH)_3$	29.67	$[Fe(OH)_3] = 10^{29.67}[Fe^{3+}][OH^-]^3$
$Fe^{3+} + SO_4{}^{2-} = Fe(SO_4)^+$	2.03	$[Fe(SO_4)^+] = 10^{2.03}[Fe^{3+}][SO_4{}^{2-}]$
$Fe^{3+} + 2SO_4{}^{2-} = Fe(SO_4)_{2-}$	2.98	$[Fe(SO_4)_2{}^-] = 10^{2.98}[Fe^{3+}][SO_4{}^{2-}]^2$
$Fe(OH)_3 = Fe^{3+} + 3OH^-$	−38.55	$[Fe^{3+}][OH^-]^3 = 10^{-38.55}$
$FePO_4 = Fe^{3+} + PO_4{}^{3-}$	−23	$[Fe^{3+}][PO_4{}^{3-}] = 10^{-23}$

The total concentrations of Fe, P, and S are expressed in Equations (3)–(5):

$$[Fe_{III}] = [Fe^{3+}] + [FeOH^{2+}] + [Fe(OH)_2{}^+] + [Fe(OH)_3] + [Fe(SO_4)^+] + [Fe(SO_4)_2{}^-] = [Fe^{3+}] + 10^{11.87}[Fe^{3+}][OH^-] + 10^{21.17}[Fe^{3+}][OH^-]^2 + 10^{29.67}[Fe^{3+}][OH^-]^3 + 10^{2.03}[Fe^{3+}][SO_4{}^{2-}] + 10^{2.98}[Fe^{3+}][SO_4{}^{2-}]^2 \quad (3)$$

$$[P] = [PO_4{}^{3-}] + [HPO_4{}^{2-}] + [H_2PO_4{}^-] + [H_3PO_4] = [PO_4{}^{3-}] + 10^{12.36}[H^+][PO_4{}^{3-}] + 10^{7.2}[H^+][HPO_4{}^{2-}]/10^{19.57}[H^+][PO_4{}^{3-}] + 10^{2.04}[H^+][H_2PO_4{}^-]/10^{21.6}[H^+]^3[PO_4{}^{3-}] \quad (4)$$

$$[S] = [SO_4{}^{2-}] + [HSO_4{}^-] + [H_2SO_4] + [FeSO_4{}^+] + 2[Fe(SO_4)_2{}^-] = [SO_4{}^{2-}] + 10^{1.93}[H^+][SO_4{}^{2-}] + 10^3[H^+][HSO_4{}^-] + 10^{2.03}[Fe^{3+}][SO_4{}^{2-}] + 2 \times 10^{2.98}[Fe^{3+}][SO_4{}^{2-}]^2 = [SO_4{}^{2-}] + 10^{1.93}[H^+][SO_4{}^{2-}] + 10^{1.07}[H^+][SO_4{}^{2-}] + 10^{2.03}[Fe^{3+}][SO_4{}^{2-}] + 2 \times 10^{2.98}[Fe^{3+}][SO_4{}^{2-}]^2 \quad (5)$$

For orthophosphate of $Mx(PO_4)y$, the relationship between $[Fe^{3+}]$ and pH is as follows:

$$\lg[Fe^{3+}] = -12.9 + 0.5\lg(1 + 4.8 \times 10^{21-3pH} + 3.6 \times 10^{19-2pH} + 2.3 \times 10^{12-pH}) \quad (6)$$

For hydroxides of $Fe(OH)_3$, the relationship between $[Fe^{3+}]$ and pH is:

$$\lg[Fe^{3+}] = 4.6-3pH \quad (7)$$

The above two formulas represent the relationship between the molar concentration of the dissolution equilibrium ion and the pH change in $FePO_4$ and $Fe(OH)_3$, respectively. In the same way, the equilibrium system curve of the molar concentration and the pH value of Mn^{2+}, Mg^{2+}, Ca^{2+}, Al^{3+}, Fe^{3+}, and other metal ions can be obtained, as shown in Figures 3 and 4.

3.1.2. lg(M^{n+})-pH Diagram of the Reaction Solution System

According to Figure 3, the precipitation sequence of orthophosphate is $FePO_4{\cdot}2H_2O$, $AlPO_4{\cdot}nH_2O$, $Mn_3(PO_4)_2{\cdot}nH_2O$, $Ca_3(PO_4)_2$, and $Mg_3(PO_4)_2{\cdot}8H_2O$. Meanwhile, the precipitation sequence of hydroxides is $Fe(OH)_3$, $Al(OH)_3$, $Mn(OH)_2$, $Mg(OH)_2$, and $Ca(OH)_2$.

In order to observe the critical pH value of each orthophosphate and hydroxide in the system more intuitively, the part in Figure 3 is enlarged to obtain Figure 4. As shown in Figure 4, the precipitation sequence of each orthophosphate and hydroxide under different reaction pH conditions can be intuitively obtained. Combined with the concentration of each metal ion in titanium dioxide waste acid, the pH value of metal ions forming orthophosphate and hydroxide precipitation in the solution can be calculated, as shown in Table 2.

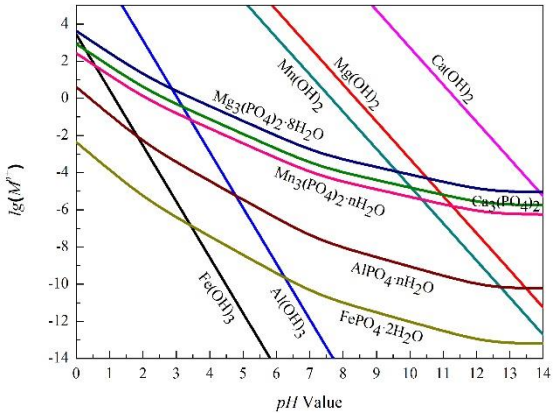

Figure 3. Relationship between lg(M^{n+}) and pH.

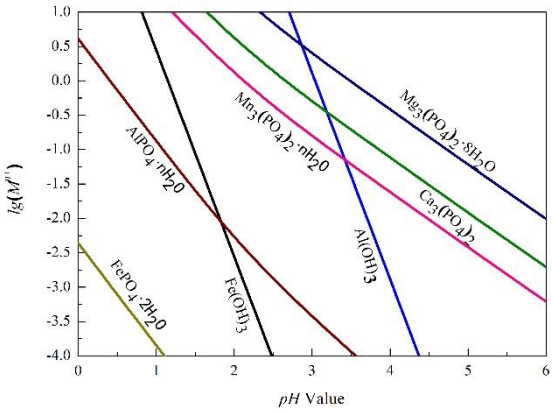

Figure 4. Enlarged view of lg(M^{n+})-pH relationship.

It can be seen from Table 4 that iron phosphate precipitates preferentially to other metal ions when pH = 0–2. Meanwhile, with the increase of pH, a small amount of aluminum ions will also form aluminum phosphate precipitate. Since iron ions preferentially form iron phosphate, there is little iron hydroxide in this pH range. When continuing to increase the pH value of the solution, magnesium and manganese ions will gradually form a corresponding phosphate precipitation.

Table 4. Critical pH of each phosphate and hydroxide precipitation in the reaction system.

Metal Ion	Mn^{2+}	Mg^{2+}	Ca^{2+}	Fe^{3+}	Al^{3+}
$lg[M^{n+}]$	0.33	0.70	−0.64	1.58	0.18
Initial precipitation pH of orthophosphate	1.8	2.6	3.4	<0	0.3
Initial precipitation pH of hydroxide	7.5	8.0	11.7	0.6	3.0

3.2. *Effect of Reaction Temperature*

The experimental conditions were set as follows: pH = 2, molar ratio of P/Fe = 1:1, reaction time of 25 min, standing for 1 h, and roasting at 700 °C for 8 h. The effects of temperatures of 40, 50, 60, and 70 °C on the precipitation process were investigated. The precipitated phases and related experimental results are shown in Figures 5 and 6.

In Figure 5, when the reaction temperature is 40–70 °C, the precipitate obtained is mainly iron phosphate, and only a small amount of aluminum forms aluminum phosphate, which is consistent with the results of the thermodynamic analysis. Meanwhile, with the gradual increase of the precipitation temperature, the crystal form and peak strength base of $FePO_4$ after calcination are not affected, and the crystal form of the product is hexagonal after analysis.

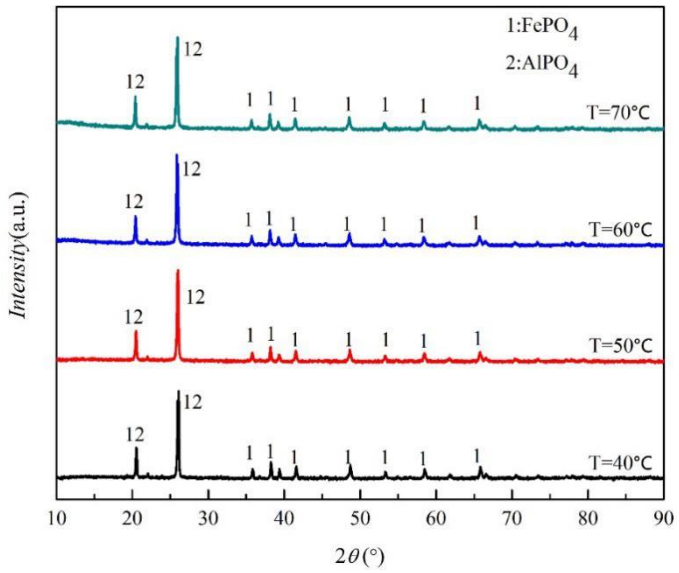

Figure 5. XRD pattern of the sample at different reaction temperatures.

As seen in Figure 6, the utilization ratios of iron and phosphorus increase from 84.44% to 97.12% and from 88.63% to 97.16%, respectively, with the temperature rising from 40 °C to 60 °C. Furthermore, with the temperature continuing to rise to 70 °C, the utilization ratios of iron and phosphorus decrease to 93.24% and 93.23%, separately. In general, the increase of the precipitation temperature will increase the reaction rate, which matches the experimental results of 40–60 °C. However, when the temperature is over 60 °C, the decrease of the percent yield is due to the agglomeration of the precipitated products, and the further precipitation is affected.

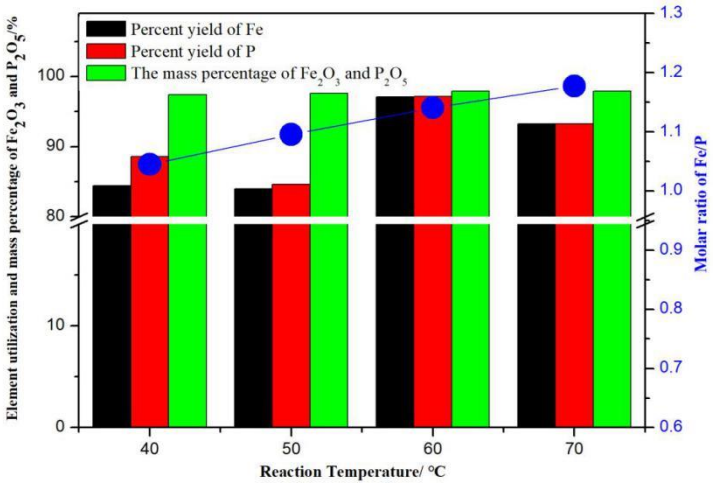

Figure 6. The effect of the reaction temperature on the utilization ratio of the elements/purity and the molar ratio of Fe/P in iron phosphate.

Moreover, in the investigated temperature range, the mass percentage of Fe_2O_3 and P_2O_5 and the molar ratio of Fe/P in the precipitate slowly increase from 97.44% and 1.04 at 40 °C to 97.88% and 1.17 at 70 °C. In conclusion, the optimal reaction temperature is set as 60 °C.

3.3. *Effect of Initial pH Value*

The experimental conditions were set as follows: reaction temperature of 60 °C, molar ratio of P/Fe = 1:1, reaction time of 25 min, standing for 1 h, and roasting at 700 °C for 8 h. The effects of pH values of 1.5, 2.0, 2.5, 3.0, and 3.5 on the precipitation process were investigated. The precipitated phases and related experimental results are shown in Figures 7 and 8.

As can be seen from Figure 7, when the pH = 1.5–3, the main component of the product is $FePO_4$, along with a part of $AlPO_4$ being generated. Moreover, when the pH rises to 3.5, a new phase of $Mg_{1.5}Fe_{1.5}(PO_4)_2$ is formed in the product, which is consistent with the thermodynamic data in Table 4. Moreover, with the increase of pH, the peak strength of the product also decreases. In particular, when pH > 2.5, the peak strength decreases sharply.

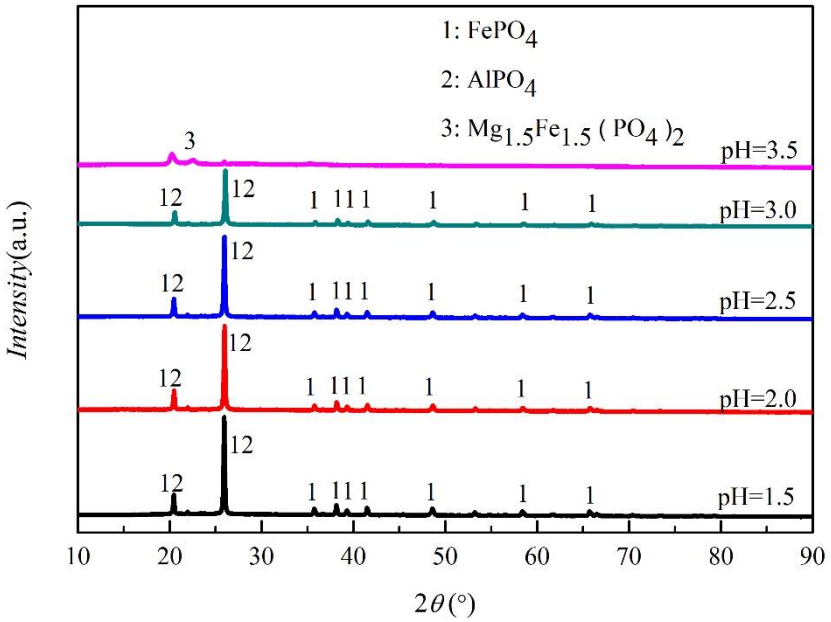

Figure 7. XRD pattern of the sample at different pH values.

In Figure 8, when the pH value of the solution increases from 1.5 to 2.5, the utilization ratios of iron and phosphorus increase from 47.23% to 97.53% and from 53.57% to 98.46%, respectively. Additionally, when the pH value increases to 3.0, the utilization ratios of iron and phosphorus basically remain unchanged. The utilization ratios of iron and phosphorus increase with pH increasing in the range of 1.5–3.0, The experimental result is consistent with the deprotonation of phosphate ions in this pH range (PKa1 of H_3PO_4 is 2.15), which causes a decrease in the equilibrium concentration of iron as the pH rises, and hence increases utilization. In addition, within the whole pH value range, the mass percentage of Fe_2O_3 and P_2O_5 basically remains unchanged at 98%. Meanwhile, the molar ratio of Fe/P in the precipitate slowly increases from 1.07 to 1.11. To sum up, the optimal pH value is set as 2.5.

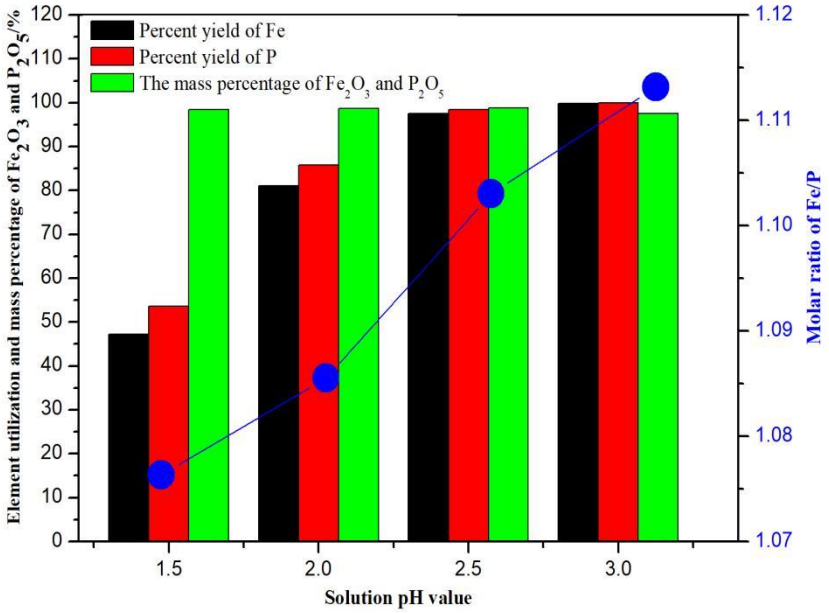

Figure 8. The effect of the initial pH value on the utilization ratio of the elements/purity and the molar ratio of Fe/P in iron phosphate.

3.4. Effect of Molar Ratio of P/Fe

The experimental conditions were set as follows: reaction temperature of 60 °C, pH value of 2.5, reaction time of 25 min, standing for 1 h, and roasting at 700 °C for 8 h. The effects of molar ratios of P/Fe of 1.0, 1.1, 1.2, 1.3, and 1.4 on the precipitation process were investigated. The precipitated phases and related experimental results are shown in Figures 9 and 10.

In Figure 9, the precipitate phase is still dominated by iron phosphate, with a small amount of $AlPO_4$ when the molar ratio of P/Fe ranges from 1 to 1.4. Additionally, with the increase of the molar ratio, the peak strength of the product decreases accordingly.

As shown in Figure 10, when the molar ratio of P/Fe increases from 1.0 to 1.1, the utilization ratio of iron and phosphorus basically remains unchanged at about 98%. Continuing to increase the molar ratio from 1.1 to 1.4, the utilization ratio of iron decreases slightly from 98.81% to 97.06%, and the utilization ratio of phosphorus decreases greatly from 98.39% to 91.54%. Moreover, the mass percentage of Fe_2O_3 and P_2O_5 remains unchanged at 99% for the whole range of the molar ratio, and the ratio of Fe/P in the precipitate decreases slowly from 1.10 to 0.91.

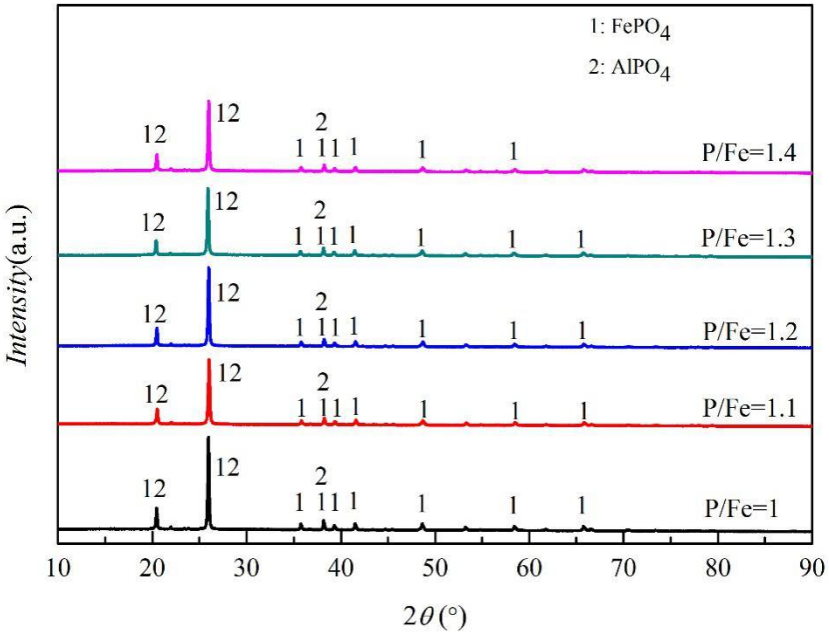

Figure 9. XRD pattern of samples at different molar ratios of P/Fe.

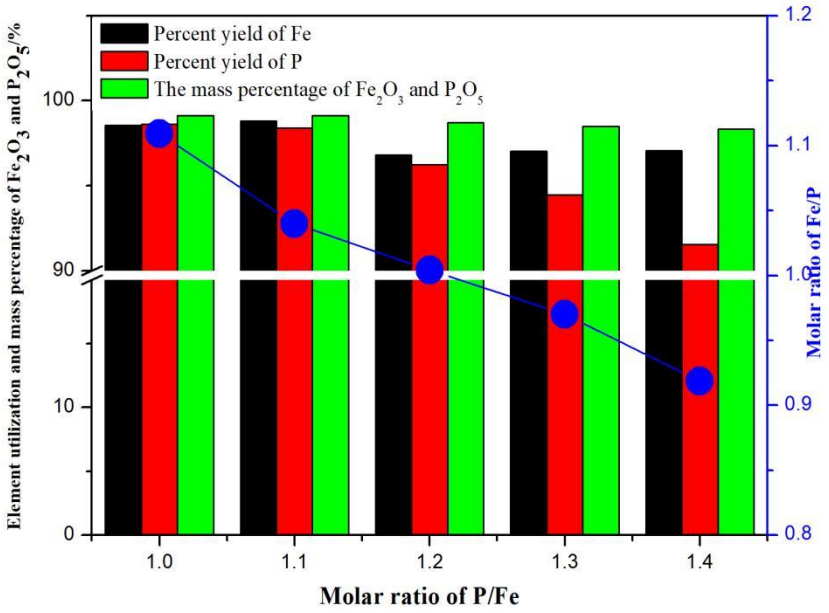

Figure 10. The effect of the molar ratio of P/Fe in solution on the utilization ratio of the elements/purity and the molar ratio of Fe/P in iron phosphate.

The increase of the molar ratio of P/Fe in the feed solution entails the increase of the precipitant phosphoric acid. Therefore, with the increase of the molar ratio, the utilization ratio of phosphorus decreases with the increase of total phosphorus. In addition, the reason for the decrease of the iron percent yield is that the increase of the phosphoric acid content leads to the aggregation of precipitated products, which leads to the decrease of the precipitation rate and iron utilization rate. In conclusion, the optimal ratio of P/Fe is selected as 1.1.

3.5. Effect of Dispersant

In order to make the dispersion of the precipitated product iron phosphate better, the effect of polyethylene glycol on the precipitation process was investigated. As a kind of mature dispersant, polyethylene glycol can weaken the bonding between hydroxyl (-OH) and the particle surface,

thus weakening the surface tension and agglomeration between particles, and limiting the growth of particles.

The experimental conditions were set as follows: pH = 2, molar ratio of P/Fe = 1.1, temperature of 60 °C, reaction time of 25 min, standing for 1 h, and roasting at 700 °C for 8 h. The effects of polyethylene glycol at 5, 10, 15, and 20 mL (per 50 mL of waste acid) on the precipitation process were investigated. The experimental results of the phase, morphology, and particle size analysis of the precipitates are shown in Figures 11 and 12, and in Table 5.

It can be seen from Figure 11 that with the increase of PEG addition, the peak strength of the precipitated iron phosphate does not change significantly. Therefore, we know that PEG addition is better at changing the dispersibility and reducing the particle size of the sample, but also that it has no effect on the peak strength of the product without introducing new impurities.

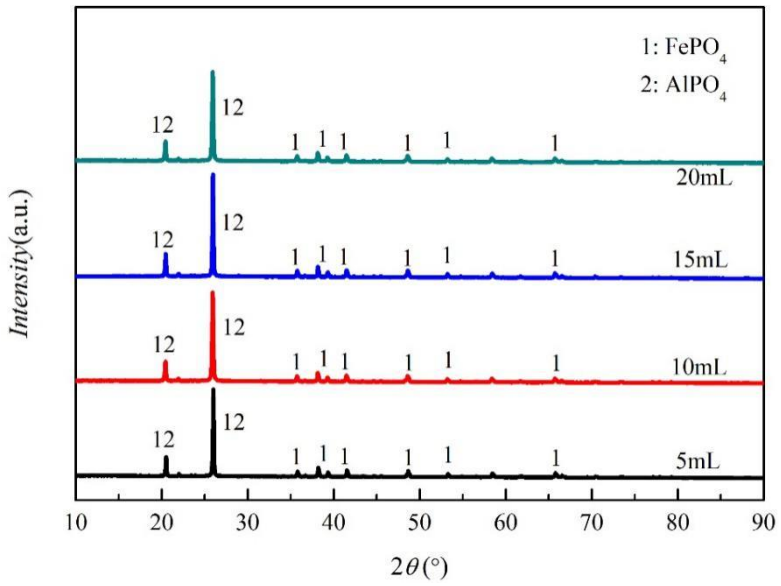

Figure 11. XRD patterns of the samples at different dosages of polyethylene glycol.

In Figure 12, with an increased amount of polyethylene glycol added into the reaction system (from a to d), the dispersibility of the sample begins to increase significantly. Meanwhile, it becomes looser, and the particle size becomes finer and finer, which can greatly increase the specific surface area of the sample and improve the product performance. Moreover, it can be seen from Table 5 that the particle size of the product decreases with the increase of PEG from 0 mL to 20 mL. D50 decreases from 17.28 μm to 4.8 μm, D90 decreases from 47.32 μm to 26.42 μm, and the volume average diameter decreases from 21.39 μm to 10.00 μm.

It can be seen that not only does polyethylene glycol not change the phase of precipitated products, but it also greatly increases the dispersion and reduces the particle size of products. In order not to reduce the percent yield of the elements and the mass percentage of Fe_2O_3 and P_2O_5 in the products, we choose 5 mL as the appropriate amount of polyethylene glycol.

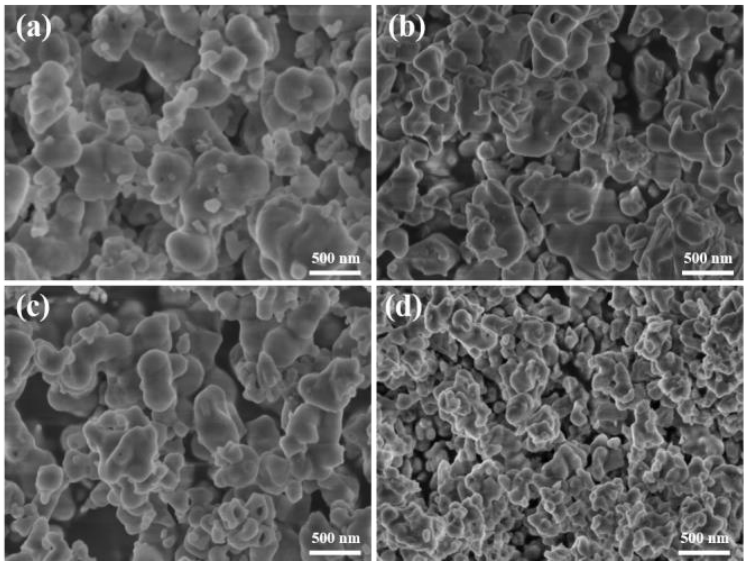

Figure 12. Effect of polyethylene glycol on the microstructure of the sample. (**a**) 5 mL; (**b**) 10 mL; (**c**) 15 mL; and (**d**) 20 mL.

Table 5. Particle size distribution of the sample when adding polyethylene glycol.

Amount of Polyethylene Glycol	Particle Size		
	D50/μm	D90/μm	Volume Average Diameter/μm
V = 0 mL	17.28	47.32	21.39
V = 5 mL	8.61	34.75	14.00
V = 10 mL	5.36	34.56	12.75
V = 15 mL	5.89	27.81	10.93
V = 20 mL	4.83	26.42	10.00

4. Conclusions

The thermodynamics and experimental results of the preparation of doped iron phosphate precursor via the selective precipitation of iron in titanium dioxide waste acid are as follows:

(1) The thermodynamics results show that iron(II) in titanium dioxide waste acid is oxidized and is preferentially precipitated with phosphoric acid to form iron(III) phosphate, when compared with other impurity ions; furthermore, the pH value of the iron phosphate precipitation is much lower than that of other impurities and slightly lower than that of aluminum ion.

(2) The experimental results show that the optimal precipitation condition is a temperature of 60 °C, an initial pH value of 2.5, an optimal P/Fe molar ratio of 1.1, and a dispersant polyethylene glycol at 5 mL (per 50 mL of waste acid). After calcination, the precipitate mainly consists of iron phosphate and a small amount of aluminum phosphate. In addition, the utilization ratios of iron and phosphorus are 98.81% and 98.39%, respectively. Meanwhile, the mass percentage of Fe_2O_3 and P_2O_5 and the molar ratio of iron to phosphorus are 99.13% and 1.03, which basically meets the requirements of the iron phosphate precursor.

Author Contributions: Writing-original draft, W.Z.; writing-review & editing, T.-a.Z.; resources, L.C.; writing—review & editing, G.L.; writing-review & editing, X.C. All authors have read and agreed to the published version of the manuscript.

Funding: This work was supported by the Fundamental Research Funds for the Central Universities (N182504018), the National Natural Science Foundation of China (Nos.51874078), the Fund of Liaoning S&T Project (20180551008)

Acknowledgments: The authors would like to thank Laboratory Center of Northeastern University for analysis.

Conflicts of Interest: The authors declare no conflict of interest.

References

1. Xu, H.; Fu, M. Research process in comprehensive utilization of spent acid and waste water in titanium dioxide production. *Multipurp. Util. Miner. Resour.* **2006**, *4*, 34–37.
2. Li, L. Research Progress on Comprehensive Recycle of Waste Acid in Titanium Pigment Production at Home and Abroad. *Hydrometall. China* **2010**, *29*, 150–155.
3. Pei, R. *Production of Titanium Dioxide by Sulfuric Acid Method*; Chemical Industry Press: Beijing, China, 1982; pp. 272–275.
4. Zhao, Y.; Zhang, Y.; Xing, W.; Xu, N. Treatment of titanium white waste acid using ceramic microfiltration membrane. *Chem. Eng. J.* **2005**, *111*, 31–38. [CrossRef]
5. Feng, X.; Jiang, L.; Song, Y. Titanium white sulfuric acid concentration by direct contact membrane distillation. *Chem. Eng. J.* **2016**, *285*, 101–111. [CrossRef]
6. Xu, T.; Yang, W. Sulfuric acid recovery from titanium white (pigment) waste liquor using diffusion dialysis with a new series of anion exchange membranes—Static runs. *J. Membr. Sci.* **2001**, *183*, 193–200.
7. Zhang, T.; Lv, G.; Liu, Y.; Zhang, G. A Comprehensive Utilization Method of Titanium White Waste Acid. CN Patent 104178632 B, 22 June 2016.
8. Zhang, T.; Zhang, W.; Lv, G.; Dou, Z.; Liu, Y. A Method of Treating Titanium White Waste Acid by Steel Slag. CN Patent 201810288264.X, 14 September 2018.
9. Zhang, T.; Lv, G.; Dou, Z.; Liu, Y.; Zhang, W. A Method of Treating Titanium White Waste Acid with Steel Slag and Extracting Valuable Components. CN Patent 201810296696.5, 14 September 2018.
10. Zhang, W.; Zhang, T.; Lv, G.; Zhou, W. Extraction Separation of Sc(III) and Fe(III) from a Strongly Acidic and Highly Concentrated Ferric Solution by D2EHPA/TBP. *JOM* **2018**, *70*, 2837–2845. [CrossRef]
11. Zhang, Y.; Zhang, T.; Dreisinger, D.; Lv, C.; Lv, G.; Zhang, W. Recovery of vanadium from calcification roasted-acid leaching tailing by enhanced acid leaching. *J. Hazard. Mater.* **2019**, *369*, 632–641. [CrossRef]
12. Zhang, G.; Zhang, T.; Zhang, Y.; Lv, G.; Liu, Y.; Liu, Z. Pressure leaching of converter vanadium slag with waste titanium dioxide. *Rare Met.* **2016**, *35*, 576–580. [CrossRef]
13. Wu, L.; Li, X.; Wang, Z. A novel process for producing synthetic rutile and $LiFePO_4$ cathode material from ilmenite. *J. Alloy. Compd.* **2010**, *506*, 271–278. [CrossRef]
14. Wu, L.; Li, X.; Wang, Z. Preparation of synthetic rutile and metal-doped $LiFePO_4$ from ilmenite. *Powder Technol.* **2010**, *199*, 293–297. [CrossRef]
15. Fan, Q.; Lei, L.; Xu, X. Direct growth of $FePO_4$/graphene and $LiFePO_4$/graphene hybrids for high rate Li-ion batteries. *J. Power Sources* **2014**, *257*, 65–69. [CrossRef]
16. Prosini, P.; Lisi, M.; Scaccia, S. Synthesis and characterization of amorphous hydrated $FePO_4$ and its electrode performance inlithium batteries. *J. Electrochem. Soc.* **2002**, *149*, A297–A301. [CrossRef]
17. Liu, H. Synthesis of nanorods $FePO_4$ via a facile route. *J. Nanopart. Res.* **2010**, *12*, 2003–2006. [CrossRef]
18. Kahoul, A.; Hammouche, A. Electrochemical performances of $FePO_4$-positive active mass prepared through a new sol-gel method. *Ionics* **2010**, *16*, 105–109. [CrossRef]
19. Wu, Y.; Chen, L.; Xie, K. Synthesis and characterization of multi–wall carbon nanotubes supported-hydrated iron phosphate cathode material for lithium–ion cells by a novel homogeneous precipitation method. *Ionics* **2012**, *18*, 721–729. [CrossRef]
20. Wang, Y.; Chen, F.; Ma, X.; Zhang, G. Recovery of nitric and acetic acids from etching waste solution using a synergistic system of N235 and TRPO in cyclohexane. *Hydrometallurgy* **2019**, *185*, 23–29. [CrossRef]
21. Chen, F.; Wang, X.; Liu, W. Selective extraction of nitric and acetic acids from etching waste acid using N235 and MIBK mixtures. *Sep. Purif. Technol.* **2016**, *169*, 50–58. [CrossRef]
22. Li, C.; Li, G.; Guo, H. Synthesis of FePO4 by electrolyzing ferrophosphorus. *Phosphate Compd. Fertil.* **2014**, *29*, 13–15.
23. Yang, J.; Lv, N.; Su, C. Research progress on the recycling of phosphorus resource from converter steelmaking slag. *Appl. Chem. Ind.* **2019**, *48*, 1440–1446.
24. Li, H.; Xing, S.; Liu, Y. Recovery of Lithium, Iron, and Phosphorus from Spent LiFePO4 Batteries Using Stoichiometric Sulfuric Acid Leaching System. *ACS Sustain. Chem. Eng.* **2017**, *5*, 8017–8024. [CrossRef]
25. Speight, J.G. *Lange's Handbook of Chemistry*; McGRAW-HILL: New York, NY, USA, 2004.
26. Xiao, C.; Xiao, L.; Gao, C. Thermodynamic study on removal of magnesium from lithium chloride solutions using phosphate precipitation method. *Sep. Purif. Technol.* **2015**, *156*, 582–587. [CrossRef]

27. He, L.; Xu, W.; Song, Y.; Liu, X.; Zhao, Z. Selective removal of magnesium from a lithium-concentrated anolyte by magnesium ammonium phosphate precipitation. *Sep. Purif. Technol.* **2017**, *187*, 214–220. [CrossRef]
28. Xiao, C.; Zeng, L.; Wei, J.; Xiao, L.; Zhang, G. Thermodynamic analysis for the separation of tungsten and aluminium in alkaline medium using solvent extraction. *Hydrometallurgy* **2017**, *174*, 91–96. [CrossRef]
29. Zhang, W.; Zhang, T.; Lv, G. Thermodynamic study on the V(V)-P(V)-H2O system in acidic leaching solution of vanadium-bearing converter slag. *Sep. Purif. Technol.* **2019**, *218*, 164–172. [CrossRef]